Journal of Colloid and Interface Science 634 (2023) 610–620

Contents lists available at ScienceDirect

Journal of Colloid and Interface Science

journal homepage: www.elsevier.com/locate/jcis

Nanolatex architectonics: Influence of cationic charge density and size on their adsorption onto surfaces with a 2D or 3D distribution of anionic groups

Alexandros Efraim Alexakis [a,b], Maria Rosella Telaretti Leggieri [a], Lars Wågberg [c], Eva Malmström [a,b], Tobias Benselfelt [c,d,*]

[a] KTH Royal Institute of Technology, School of Engineering Sciences in Chemistry, Biotechnology and Health, Department of Fibre and Polymer Technology, Division of Coating Technology, Teknikringen 56-58, SE-100 44 Stockholm, Sweden
[b] Wallenberg Wood Science Center, Department of Fibre and Polymer Technology, KTH Royal Institute of Technology, Teknikringen 56-58, SE-100 44 Stockholm, Sweden
[c] KTH Royal Institute of Technology, School of Engineering Sciences in Chemistry, Biotechnology and Health, Department of Fibre and Polymer Technology, Division of Fibre Technology, Teknikringen 56-58, SE-100 44 Stockholm, Sweden
[d] School of Materials Science and Engineering, Nanyang Technological University, 639798 Singapore, Singapore

GRAPHICAL ABSTRACT

The polymerization of the pre-formed hydrophilic block followed by the chain extension with a hydrophobic monomer in water and the final formation and adsorption of nanolatexes onto surfaces with a 2D or 3D distribution of charged groups.

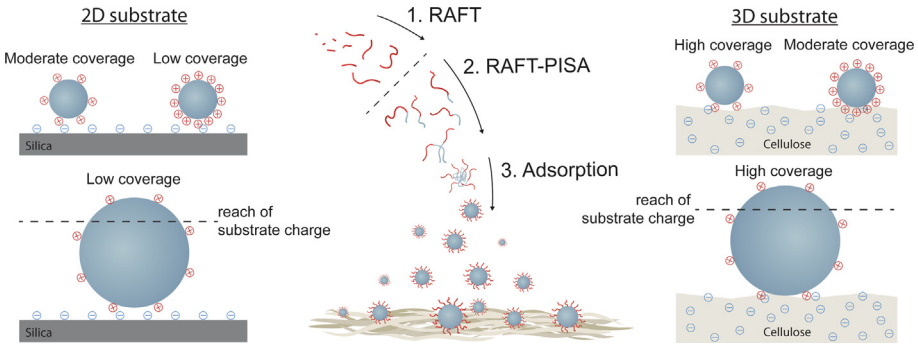

ARTICLE INFO

Article history:
Received 20 July 2022
Revised 1 December 2022
Accepted 8 December 2022
Available online 14 December 2022

Keywords:
Adsorption
TEMPO-oxidation
Cellulose
Nanolatex

ABSTRACT

Hypothesis: It is theoretically predicted and hypothesized that the charge density and size of spherical nanoparticles are the key factors for their adsorption onto oppositely charged surfaces. It is also hypothesized that the morphology and charge of the surface are of great importance. In-plane 2D (silica) or a volumetric 3D (regenerated TEMPO-oxidized cellulose model surfaces) distribution of charged groups is expected to influence charge compensation and, thus, the adsorption behavior.
Experiments: In this work, self-stabilized nanolatexes with a range of cationic charge densities and sizes were synthesized through reversible addition – fragmentation chain-transfer (RAFT) polymerization coupled with polymerization-induced self-assembly (PISA). Their adsorption onto silica and anionic cellulose model surfaces was investigated using stagnation point adsorption reflectometry (SPAR) and quartz crystal microbalance with dissipation (QCM-D).

* Corresponding author at: KTH Royal Institute of Technology, School of Engineering Sciences in Chemistry, Biotechnology and Health, Department of Fibre and Polymer Technology, Division of Fibre Technology, Teknikringen 56-58, SE-100 44 Stockholm, Sweden.
E-mail address: bense@kth.se (T. Benselfelt).

https://doi.org/10.1016/j.jcis.2022.12.038

RAFT
PISA
QCM-D
SPAR
Colloid

Findings: Experiments and theory agree and show that the size of the nanolatex and the difference in charge density compared to the substrate determine the charge compensation and, thus, the surface coverage. Highly charged or large nanolatexes overcompensate the surface charge of non-porous substrates leading to a significant repulsive zone where other particles cannot adsorb. For porous substrates like cellulose, the vertical distribution of charged groups in the 3D volume prevents overcompensation and thus increases the adsorption. This systematic study investigates the isolated effect of surface charge and size and paves the way for on-demand particles specifically designed for a surface with particular characteristics.

1. Introduction

Cellulose plays an essential role in the increasing demand for composites based on polymers derived from renewable resources.[1] Exhibiting excellent mechanical properties and wide versatility, cellulose fibrils and their derivatives from different raw materials are excellent candidates as matrices and fillers for different applications. [2,3] However, incompatibility with hydrophobic polymers, usually used in biocomposites, limits cellulose from being the material of choice. Therefore, it is essential to modify cellulose surfaces to make them more compatible with synthetic polymers. The large number of polar groups accessible on the surface of cellulosic fibers have been the primary target for chemical modification by covalent attachment, such as grafting from and grafting to. [4] Another versatile approach employed to tackle incompatibility issues is the physical adsorption (physisorption) of compatibilizers such as colloidal nanoparticles or polymers/polyelectrolytes onto cellulose-based materials. [5–9].

Theoretical predictions have stressed the importance of studying the effect of size and surface charge in the adsorption of colloidal nanoparticles onto different substrates. [9–11] However, experimental investigations are needed to validate the predicted behaviors. So far, the coupling between charge density and size for rigid particles has been a practical obstacle. [12–16] Therefore, model systems with tailored surface charge and size, as demonstrated in this work, are needed to study adsorption behaviors.

Within this scope, self-stabilized nanolatexes synthesized via reversible addition-fragmentation chain-transfer (RAFT) polymerization coupled with polymerization-induced self-assembly (PISA) offers an elegant, modular and environmentally friendly approach. [17–20].

During PISA, a pre-formed well-defined hydrophilic polymer is chain-extended in water with a hydrophobic monomer forming an amphiphilic diblock copolymer. At a critical ratio between the hydrophilic and the hydrophobic blocks, the polymers instantaneously self-assemble into micelle-like structures. Nanolatexes produced through RAFT-mediated PISA exhibit a wide variety of properties. Their size can be varied (20–200 nm), as well as their shape (sphere, worm, vesicle, etc.), charge density (100–1000 μm ol/g) and overall chemistries. [21] The tunable charge of the hydrophilic shell decouples the surface charge density from the volume of the particles enabling isolated variation of charge density and size of the nanolatexes. This method is preferable to conventional emulsion polymerization as it ensures that the stabilizing groups are covalently attached to the surface of the nanolatexes, and furthermore it does not require surfactants that might interfere with the adsorption process.

For instance, spherical xyloglucan-decorated nanolatexes with a high glass transition temperature (T_g) core polymer, poly(methyl methacrylate) (PMMA), have been utilized in the modification of cellulose filter paper. [22] However, the lacking size control and polydispersity of the formed colloids is challenging considering the polydispersed structure of xyloglucan. For this reason, ionically charged nanolatexes display a more suitable option. [14,23] Cationically charged nanolatexes comprised of a poly(2-(dimethylamino)ethyl methacrylate) (PDMAEMA) shell and a PMMA core have been used for adsorption onto cellulose filter paper targeting hydrophobization as compatibilizers in nanocellulose biocomposites. [14,15] Although in the studies discussed above, the concept of adsorbing nanolatexes on either cellulose or nanocellulose was investigated, there is still a lack of experimental evidence that support theoretical predictions regarding the in-depth understanding of the critical parameters that govern the adsorption behavior of nanolatexes onto cellulose or other softer surfaces. In particular, the size and charge density of the nanolatexes as the adsorption is driven by charge exchange, [24] and the morphology of the substrate; silica and cellulose having 2D and 3D distribution of anionic groups, respectively, so that their effective charge per area is vastly different. In this work, cationically charged nanolatexes comprised of PDMAEMA and PMMA were synthesized via RAFT-mediated PISA. These model nanolatexes are well-suited to investigate their interactions with charged cellulose and understand their structure–property relationship. By tailoring the number of repeating units of the shell and the core polymers, the size and charge density can be decoupled, and their influence on adsorption can be individually studied.

An approach to studying the adsorption of polymers and nanolatexes to cellulose is through reflectometric and gravimetric techniques because both reflectivity and mass of the substrate are affected by the adsorption process. Stagnation point adsorption reflectometry (SPAR) and quartz crystal microbalance with dissipation (QCM-D) are commonly used, provided that well-defined model surfaces can be prepared. [25,26] The main advantage of combining these techniques is that they complement each other to provide a holistic perspective on the adsorption mechanism. QCM-D measures the adsorbed amount of polymer, including the associated water, whereas SPAR only measures the adsorbed amount of polymer, and together they describe the conformation of polymers at the interface. For semi-rigid particles, this combination can primarily describe the amount of water the particles bring to the surface or deswelling of a swollen substrate. [10,27] Here, the adsorption of the prepared nanolatexes was investigated by SPAR and QCM-D, using silica and regenerated TEMPO-oxidized cellulose model surfaces (Fig. 1). These substrates are models for anionically charged non-porous (in-plane charge distribution) and porous (volumetric charge distribution) substrates.

Finally, the adsorbed nanolatexes were subjected to heat treatment (annealing) to allow the coalescence of the nanolatexes and to create a hydrophobic layer, further investigated by field emission scanning electron microscopy (FE-SEM) and contact angle measurements against water. The results of the current study will contribute to the fundamental understanding of the adsorption of well-defined charged nanolatexes onto charged surfaces and the influence of the particle size and charge density, in particular, findings that may guide to the identification of the optimal nanolatex for a targeted modification.

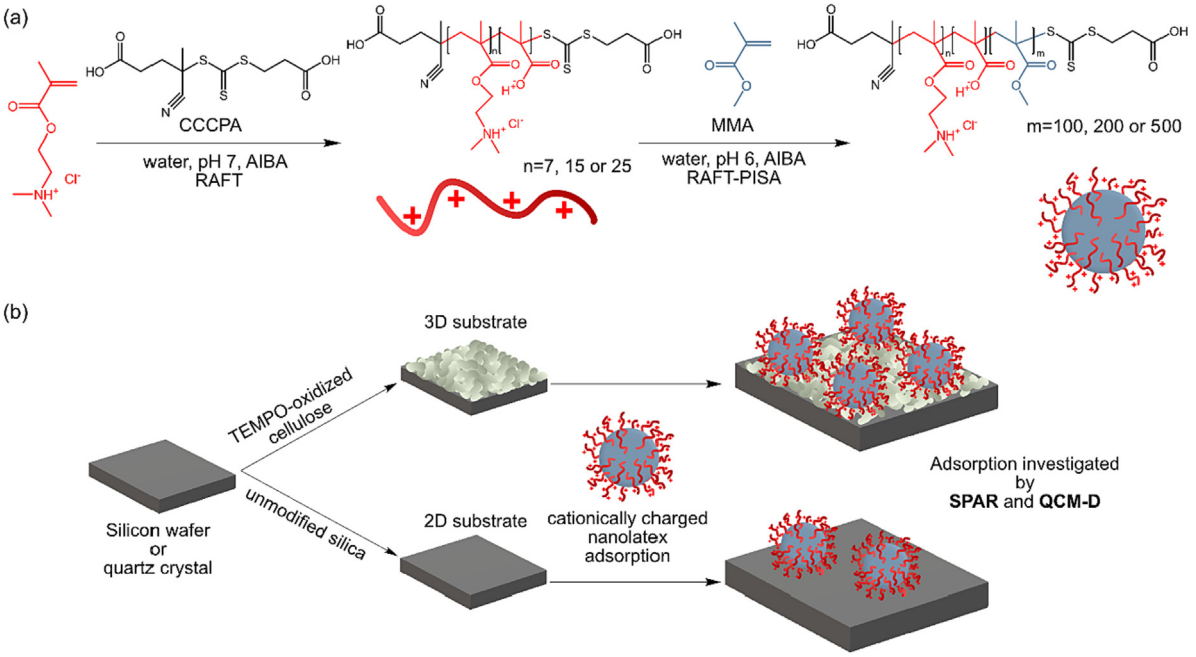

Fig. 1. Schematic representation of (a) the synthesis of cationically charged nanolatexes via RAFT-mediated PISA and (b) their adsorption onto silica and regenerated TEMPO-oxidized cellulose substrates.

2. Materials and methods

2.1. Materials

4-((((2-Carboxyethyl)thio)carbonothioyl)thio)-4 cyanopentanoic acid (CCCPA, 95 %) was purchased from Boron Molecular and used as received. 2,2′-Azobis(2-methylpropionamidine) dihydrochloride (AIBA, 97 %), 2-(dimethylamino)ethyl methacrylate (DMAEMA, 98 %), methyl methacrylate (MMA, 99 %), 4-methylmorpholine *N*-oxide (NMMO, 50 wt% H_2O solution), sodium hydroxide (NaOH, ≥98 %), sodium chlorite ($NaClO_2$, puriss. p.a., 80 %) and 2,2,6,6-tetramethylpiperidine 1 oxyl (TEMPO, ≥98 %) were all purchased from Sigma Aldrich and used as received. Hydrochloric acid (HCl, 37 wt%, AnalaR NORMAPUR®), dimethyl sulfoxide (DMSO, ≥99.9 %), ethanol (EtOH, 96 %), dimethyl sulfoxide-d_6 (DMSO d_6, 99.9 %), deuterium oxide (D_2O, 99.9 %) and sodium hypochlorite (NaClO, 14 % Cl_2 in aqueous solution, GPR RECTAPUR®) were purchased from VWR. The water used was deionized or, when specified, Milli-Q (18.2 MΩ·cm, Millipore Milli-Q Purification System). Poly(vinyl amine) (PVAm) in water solution (Lupamin 9095) was kindly supplied by BASF, Sweden. Never-dried softwood dissolving pulp fibers were kindly supplied by Domsjö Fabriker AB, Örnsköldsvik, Sweden. Silicon coated quartz crystals were purchased from Biolin Scientific (Qsense® QSX 303 Silicon dioxide, surface roughness < 1 nm). Silicon wafers were purchased from TOPSIL (RFQ of 150 mm / SZ / 1–0-0 / BORON / P type / Resis 4–6 Ohm / Thick 610–640 / Oxy 27.1–33 MIXED / 38647 + 52A0N31711E + D). Dialysis tubing with MWCO of 1 kDa and 6–8 kDa (Spectra/Por® Biotech) were purchased from VWR.

2.2. Synthetic procedures

2.2.1. TEMPO-mediated oxidation of cellulose fibers

Dissolving-grade pulp fibers, stored at 4 °C with a dry weight content of 13 wt%, anionic surface groups were added by TEMPO-mediated oxidation according to a protocol adapted from the literature. [28,29] Briefly, the fibers (15 g dry weight) were immersed in phosphate buffer (1.5 L, 0.05 M, pH 6.8) at 60 °C under magnetic stirring in an E-flask. $NaClO_2$ (0.15 mol, 13.57 g), TEMPO (1.5 μmol, 0.23 g) and NaClO (0.015 mol, 1.12 g, 0.1 M solution in phosphate buffer) were step-wise dissolved in the flask. The reaction was allowed to proceed for 140 min, and finally, the oxidized fibers were intensively washed with Milli-Q water (8 L). The charge density of the oxidized fibers was assessed by conductometric titration to be 629 ± 6 μmol/g.

2.2.2. Preparation of regenerated TEMPO-oxidized cellulose model surfaces for QCM-D and SPAR studies

Negatively charged TEMPO-oxidized cellulose model surfaces were prepared on two different types of silica surfaces used for the adsorption measurement techniques: Silicon wafers used in SPAR experiments and QCM-D crystals coated with silica. Silicon wafers were oxidized at 1000 °C for 3 h followed by consecutive rinsing with Milli-Q water, EtOH, and Milli-Q water and dried with nitrogen. The oxide layer thickness was determined by ellipsometry (43702 – 200E, Rudolph Research, Flanders NJ, U.S.A.) to be 90. 7 ± 0.4 nm. The oxidized wafers used in SPAR were cut into square pieces approximately 10 × 10 mm in size. Both oxidized wafers and QCM-D crystals were rendered hydrophilic by treatment for 2 min in a plasma cleaner (PCD 002, Harrick Scientific Corp., Ossining, NY, U.S.A.) at reduced pressure and 30 W power. After plasma treatment, the surfaces were soaked for 15 min in a solution containing 0.1 g/L poly(vinyl amine) (PVAm) with pH adjusted to 7.5 by HCl, to create an anchoring precursor layer for attachment of the cellulose. The substrates were then rinsed with Milli-Q water and dried with N_2.

Regenerated Cellulose II model surfaces were prepared onto the PVAm-treated oxidized silicon wafers and QCM-D crystals according to a procedure described in the literature. [22,23] Briefly, cellulose fibers oxidized to a charge density of 629 ± 6 μmol/g by TEMPO-mediated oxidation were dissolved first in NMMO and then DMSO was added (3:1) using rotary evaporation at 125 °C. The cellulose solution was immediately spin-coated (KW-4A-2, Chemat Technology, Northridge, CA, U.S.A.) on both substrates at 1500 rpm for 15 s and 3500 rpm for 30 s. Then, the spin-coated

substrates were immersed in Milli-Q water for 1 h, twice, to regenerate the TEMPO-oxidized cellulose. Finally, they were cured at 105 °C for 6 h and stored in the conditioning room until used.

2.2.3. RAFT polymerization of DMAEMA

The protocol used for the RAFT polymerization of DMAEMA in water has been described elsewhere. [15,30] In this study, different degrees of polymerization of PDMAEMA were prepared, i.e., 7, 15 and 25 denoted as D_7, D_{15} and D_{25}, respectively. The polymerization of D_{15} is briefly described: 4-((((2-carboxyethyl)thio)carbonothioyl)thio)-4 cyanopentanoic acid (CCCPA, 0.20 g, 0.66 mmol) and AIBA (6.3 mL (0.08 mmol) from a stock solution of 3.4 g/L in deionized water) were dissolved in 8.00 mL of water in a 25 mL round-bottom flask equipped with a magnetic stirrer. DMAEMA (1.63 mL, 9.8 mmol) was added and the pH was adjusted to 7 by adding concentrated HCl drop-wise. Then water was added to a total volume of 15.65 mL (targeting a dry content of 10 wt%). The reaction mixture was degassed with argon for 20 min while the flask was in an ice bath and then immersed in an oil bath preheated to 70 °C. The monomer conversion was monitored by ^{1}H NMR in D_2O by comparing the monomer peaks corresponding to the double bond of DMAEMA (5.7 and 6.1 ppm) with the broad polymer peak (between 0.8 and 1.2 ppm) (Figure S4-S6). After 120 min, the polymerization was quenched by letting air in and immersing the reaction flask in an ice-water bath. Then, the solution was dialyzed (MWCO 1 kDa) against deionized water for 1 day, followed by freeze-drying. The macroRAFT agent was collected as yellow solids (D_7 and D_{15}) or a yellow viscous oil (D_{25}). The final compositions of the macroRAFT agents were verified by ^{1}H NMR in D_2O where the methylene peak of the RAFT agent (2.53 ppm) was compared to the methylene polymer peak (3.49 ppm) (Figures S1-S3). As DMAEMA is slightly hydrolyzed during polymerization, the degree of hydrolysis (*DH*) was also calculated by comparing the methylene polymer peak (3.49 ppm) to the hydrolysis peak, i.e., methylene adjacent to the amine of the ethanolamine (3.20 ppm), Table 1. The detailed calculation can be found in the supporting information (equation S1). All amounts used to synthesize macroRAFT agents can be found in Table S1.

2.2.4. RAFT-mediated polymerization-induced self-assembly of MMA

The synthesis of P(DMAEMA-MMA) nanolatexes has been reported previously. [15] In the present study, the degrees of polymerization of the PMMA hydrophobic block were varied, i.e., 100, 200 and 500 denoted as M_{100}, M_{200} and M_{500} to achieve different nanolatex sizes and charge densities. The synthesis of D_{15}-M_{200} is described as an example and all experiments are listed in Table S2. D_{15} (0.216 g, 0.08 mmol) was dissolved in 15.96 mL of deionized water (targeting 10 wt% dry content) in a 25 mL round-bottom flask. An aqueous solution of AIBA (3.4 g/L) was prepared, and 0.79 mL (9.9 μmol) was added to the flask followed by the addition of MMA (1.75 mL, 16.4 mmol) while stirring. The reaction mixture was purged with argon for 20 min while in an ice bath and then transferred into an oil bath operating at 70 °C. After 120 min, the polymerization was stopped by letting air in and immersing the reaction flask in an ice-water bath. An aliquot was collected, and after freeze-drying, the dry content was calculated and correlated to conversion (equation S5). The latex dispersions were dialyzed against water for 1 day (MWCO 6–8 kDa) to remove any unreacted macroRAFT agents, and the dry content was re-evaluated. The dilution performed prior to characterizations was based on the dry content after dialysis.

2.3. Characterization techniques

2.3.1. Nuclear magnetic resonance (NMR)

The polymerization kinetics of DMAEMA for the preparation of cationic macroRAFT agents was monitored by ^{1}H NMR with a Bruker Avance AM 400 NMR instrument using D_2O as solvent (Figures S4-S6, equation S2). The degree of hydrolysis (*DH*) (Figures S1-S3, equation S1) was estimated following a previously published work. [15] All samples used for the ^{1}H NMR were freeze-dried prior to their characterization.

2.3.2. Gravimetric analysis

The final conversion of the nanolatex samples during the RAFT-mediated PISA polymerization was determined gravimetrically. Aliquots were withdrawn after 120 min, freeze-dried and weighed, yielding the dry content.

2.3.3. Differential scanning calorimetry (DSC)

DSC analysis was performed with a Mettler Toledo DSC. All freeze-dried samples were analyzed with a heating and cooling rate of 10 °C/min under a nitrogen atmosphere. The method used comprised two heating and one cooling cycle; heating from 30 to 200 °C, equilibrating for 5 min, then cooling from 200 to −20 °C, equilibrating for 5 min, and finally, a second heating ramp from −20 to 200 °C. Data from the second heating cycle were used to evaluate the glass transition temperature (T_g) for all samples.

2.3.4. Dynamic light scattering (DLS)

The hydrodynamic diameter (D_H), polydispersity index (*PdI*) and zeta potential (ζ) of the nanolatexes were determined using a Malvern Zetasizer NanoZS at ambient temperature. Each value used is the average of three consecutive measurements on the same sample. The concentration of the latex dispersions was 0.1 wt% in deionized water. The standard chosen for the size correlation of the investigated samples was polystyrene latex, set by default from the instrument.

2.3.5. Polyelectrolyte titration (PET)

The charge density of the nanolatexes was determined by polyelectrolyte titration with potassium poly(vinyl sulfate) (KPVS) as titrant in duplicate, using a Stabino unit (Particle Metrix GmbH, Germany). The concentration of nanolatexes was 0.1 wt% and the solvent used was Milli-Q water.

Table 1
Physicochemical properties of the macroRAFT agents.

Samples	*p* (%) [a]	*DH*(%) [b]	M_n(g/mol) [c]	*Charge Density (μmol/g)* [d]	T_g(°C) [e]
D_7	88	3.7	1540	996 ± 13	75.1 ± 3.9
D_{15}	91	2.0	2640	2388 ± 25	103.9 ± 6.4
D_{25}	99	0.6	4220	3095 ± 50	120.0 ± 1.5

[a] Monomer (DMAEMA) conversion calculated from equation S2.
[b] Degree of hydrolysis calculated from equation S1.
[c] Polymer molecular weight calculated from equation S4.
[d] Surface charge was measured by PET.
[e] Glass transition temperature obtained by DSC.

2.3.6. Conductometric titration (CT)

The charge density of the TEMPO-oxidized cellulose fibers was determined by conductometric titration of approximately 0.25 g pulp with 0.1 M NaOH, in duplicate, according to the SCAN-CM 65:02 protocol using a Metrohm 856 Conductivity Module. [31].

2.3.7. Field emission scanning electron microscopy (FE-SEM)

Hitachi S-4800 FE-SEM was used for imaging nanolatexes adsorbed on silica and regenerated TEMPO-oxidized cellulose model surfaces. The voltage used was set at 1 kV for all images taken. Each sample was sputtered with Pt/Pd (Cressington sputter coater 208RH) for 7 s. The nanolatex diameters were determined by the Gwyddion v2.54 software.

2.3.8. Atomic force microscopy (AFM)

The thickness of the regenerated TEMPO-oxidized cellulose model surface on silica and its roughness (Figure S18) was determined by AFM run in the tapping mode (Nanoscope III, Multimode SPM, Veeco Inc., U.S.A.). The experiment was conducted under ambient conditions and standard rectangular noncontact silicon cantilevers (RTESP, Veeco Instruments Inc., U.S.A.) were used.

2.3.9. Contact angle

Water contact angle measurements were performed using Theta Lite optical tensiometer coupled with a remote-controlled syringe (Biolin Scientific). All samples were kept for at least 24 h at 50 % RH at ambient temperature before the measurement. The sessile drop method with a volume of 4 μL was used. Images of the deposited droplet were captured every 25 ms and evaluated using the OneAttention software (Biolin Scientific) to obtain the average contact angle (θ) and hence the $cos\theta$. The baseline and the shape of the droplet, were automatically retrieved from the software. Each sample was measured in three distinct positions to check for homogeneity and increase statistics. The obtained values can be found in Figure 7 and Table S4.

2.3.10. Stagnation point adsorption reflectometry (SPAR)

The adsorption of nanolatexes on silica and regenerated TEMPO-oxidized cellulose model surfaces was monitored by SPAR (Laboratory of Physical Chemistry and Colloidal Science, Wageningen University). Detailed information about the SPAR technique can be found in the literature. [32] Briefly, a beam of linearly polarized light is focused on the stagnation point of the sample flow perpendicular to the sensor surface and reflected toward the detector. The parallel (I_p) and perpendicular (I_s) polarized light components are separated by a beam splitter and the intensity ratio ($S = \frac{I_p}{I_s}$) is determined which is proportional to the reflectivity ratio of the surface and therefore changes with the adsorption of nanolatexes. The adsorbed amount (Γ_{SPAR}) can be calculated as:

$$\Gamma_{SPAR} = A_s^{-1} \frac{\Delta S}{S_o} \quad (1)$$

where A_s^{-1} is the sensitivity factor which is proportional to the refractivity index increment with respect to concentration $\left(\frac{dn}{dC}\right)$ and S_o is the initial reading of the reflectometer. The sensitivity factors used in this study were determined by Prof. Huygens software (Dullware, The Netherlands). The $\frac{dn}{dC}$ of each nanolatex dispersion (0.139, 0.134, 0.122 and 0.136 mL/g for D_7-M_{100}, D_{15}-M_{200}, D_{15}-M_{500} and D_{25}-M_{200}, respectively) was determined by an Abbe refractometer (Carl Zeiss, Germany, Figure S15). SPAR experiments were conducted at pH 6 and ambient temperature. The flow rate was approximately 1 mL/min, and the concentration of latex dispersions was 0.025 g/L. All samples were equilibrated in deionized water until a stable baseline was reached after 30 min for silica and 1 h for regenerated TEMPO-oxidized cellulose model surfaces. The adsorption was monitored for 1 h, followed by a washing step with deionized water for an additional 30 min to ensure the adhesion of the adsorbed layer.

2.3.11. Quartz crystal microbalance with dissipation (QCM-D)

The adsorbed amount and the viscoelastic properties of the adsorbed layer of nanolatexes on silica-coated quartz crystals and regenerated TEMPO-oxidized cellulose model films were determined using QCM-D (E4 model, Q-Sense Ab, Gothenburg, Sweden). All QCM-D experiments were conducted at pH 6 and ambient temperature with a latex dispersion concentration of 0.025 g/L. All surfaces were allowed to equilibrate in deionized water until a stable baseline was achieved after 1 h for the regenerated TEMPO-oxidized cellulose model surface and 30 min for silica at a flow rate of 0.3 mL/min. The adsorption was monitored for 1 h with a 0.1 mL/min flow rate and a final washing step with deionized water of 10 min. The adsorbed amount (Γ_{QCM}) was calculated using the Sauerbrey equation [33]:

$$\Gamma_{QCM} = C\left(\frac{\Delta f}{n}\right) \quad (2)$$

where C is the sensitivity constant (-0.177 mg/m^{2}Hz), n is the overtone number (3 was used in this study) and Δf is the change in resonance frequency (Hz).

With QCM-D the viscoelastic properties can also be studied through the dissipartion factor of the adsorpbed layer:

$$D = \frac{E_{dissipated}}{2\pi E_{stored}} \quad (3)$$

where $E_{dissipated}$ is the dissipated energy of one oscillation period and E_{stored} is the stored energy in the oscillating system. Although the Sauerbrey equation is a model applied for rigid films, studies have shown that it is also valid for systems with higher dissipation and compared to more advanced viscoelastic models. [34] In addition, in the current work, the dissipation was relatively low, so the Sauerbrey equation was considered a good approximation.

3. Results and discussion

The core of this study was to investigate how the adsorption of nanolatexes on silica and regenerated TEMPO-oxidized cellulose model surfaces is affected by the size and charge density of the nanolatexes. These substrates also represent a 2D (silica) and 3D (cellulose) distribution of anionic groups, which should significantly impact the charge compensation and the resulting adsorption. The results are divided into three parts: i) The synthesis of cationically charged macroRAFT agents with different degrees of polymerization. ii) Utilization of the macroRAFT agents in the RAFT-mediated polymerization-induced self-assembly (PISA) and the characterization of the corresponding nanolatexes in the wet and dry states. iii) Adsorption of the tailored nanolatexes onto anionic silica and anionic regenerated TEMPO-oxidized cellulose model surfaces and assessment of their film-forming properties before and after annealing.

3.1. Synthesis of macroRAFT agent based on DMAEMA

The synthesis of cationically charged macroRAFT agents was pursued via RAFT polymerization of DMAEMA in water using previously published protocols (Fig. 1a). [15,30] In this work, three different degrees of polymerization (*DP*) were targeted: $PDMAEMA_7$, $PDMAEMA_{15}$ and $PDMAEMA_{25}$, referred to as D_7, D_{15} and D_{25}, where the subscript indicates the targeted *DP*. The polymerization was followed by ^{1}H NMR in D_2O (Figures S4-6) over 120 min and the conversion was calculated and plotted against the reaction

time (Figure S8). DMAEMA is partly hydrolyzed into methacrylic acid (MAA) during polymerization, resulting in a statistical copolymer. [15] All macroRAFT agents reached monomer conversion close to 90 % while keeping the degree of hydrolysis (*DH*) below 3.7 % (Table 1). Due to their polyelectrolyte character, the number average molecular weight (M_n) of resulting polymers could not be assessed by size exclusion chromatography (*SEC*). [30] Therefore, M_n was calculated through ^{1}H NMR by end-group analysis (equation S4, Table 1).

Polyelectrolyte titration (PET) was conducted to determine the charge density of the macroRAFT agents using potassium poly (vinyl sulfate) (KPVS) as titrant. The charge density followed the same trend as M_n (Table 1). By increasing the *DP*, and hence the M_n, the number of charges on the polymer was increased from 7 to 25. This increase is expressed in the charge density, where D_7 has the lowest value (~1000 μmol/g) and D_{25} has the highest (~3000 μmol/g).

The thermal properties of the macroRAFT agents were studied by differential scanning calorimetry (DSC) to determine the glass transition temperature (T_g). It was observed that by increasing M_n the T_g was increased from 75 to 120 °C, which is supported by similar works regarding quaternized PDMAEMA. [35].

3.2. RAFT-mediated PISA of MMA

Access to well-defined nanolatexes with tailored size and charge densities is critical to investigating the parameters that govern the adsorption of nanolatexes onto substrates. Hence, this part discusses the synthesis of nanolatexes with cationically charged macroRAFT agents as a stabilizing shell and hydrophobic poly (methyl methacrylate) (PMMA) as the core.

The macroRAFT agents were chain extended via controlled radical polymerization techniques with MMA in water using the polymerization-induced self-assembly (PISA) technique without further adjusting the pH (Fig. 1a). [14,15] The resulting amphiphilic diblock copolymers self-assemble in water at a critical PMMA chain length to form nanolatexes. The targeted *DPs* of PMMA, shown in subscript, were chosen to obtain nanolatexes of various sizes, e.g. $PDMAEMA_7$-$PMMA_{100}$ referred to as D_7-M_{100}.

The hydrodynamic (D_H) and dried (D_{SEM}) diameters of the nanolatexes were assessed by DLS and FE-SEM, respectively (Figure S10, Table 2). In both cases, 0.1 wt% dilutions of the nanolatex dispersion were used, and in the case of FE-SEM, the samples were spin-coated on silicon wafers (Figure S10). The nanolatexes D_7-M_{100}, D_{15}-M_{200} and D_{25}-M_{200} had comparable diameters, i.e., ~ 40 nm based on DLS and ~ 33 nm based on FE-SEM, while exhibiting different charge densities. The cationic character of the nanolatexes was supported by the positive zeta potential (ζ) listed in Table 2. These nanolatexes allowed the investigation of the effect of charge density irrespectively of size. D_7-M_{100} and D_{15}-M_{500}, with similar charge densities of ~ 330 μmol/g, were chosen to study the isolated effect of size. Charge per mass is the better unit to compare if one considers a mean field approximation of electrostatics – that is, the exact position of a charge is not that important since charges feel each other over large distances, and the size of most nanoparticles is within this distance. The same principle applies to cellulose surfaces with a 3D distribution of anionic groups.

The size polydispersity index (*PdI*) obtained from DLS demonstrated the existence of monodisperse nanolatexes as all values were below 0.1, except in the case of D_7-M_{100} (0.12). The *PdI* can also be interpreted as an indicator of control obtained during the polymerization. In this respect, complete control could not be reached for D_7-M_{100}, probably explained by the short hydrophilic block. However, FE-SEM showed a monodisperse size distribution (Figure S10).

The glass transition temperature, T_g, of each nanolatex was studied by DSC (Table 2). All nanolatexes displayed a T_g, around 125 °C, since the main influence is from the hydrophobic PMMA-core (Table 1). The theoretical T_g-values calculated by the Flory-Fox equation (equation S6) assuming homogeneous mixing were approximately 20 °C lower than the experimentally obtained T_g (*SI* part 5).

3.3. Adsorption of nanolatexes onto silica and regenerated TEMPO-oxidized cellulose model surfaces

The adsorption of the cationically charged nanolatexes onto anionic non-porous silica (in-plane 2D charge distribution) and porous (volumetric 3D charge distribution) regenerated TEMPO-oxidized cellulose model surfaces is discussed in detail in this section. The adsorption was monitored by Stagnation Point Adsorption Reflectometry (SPAR) and Quartz Crystal Microbalance with Dissipation (QCM-D). After that, the film formation properties before and after annealing were investigated using FE-SEM and contact angle measurements.

Model substrates are needed to study the parameters that influence the adsorption of nanolatexes. For this reason, silica was used as a reference non-porous substrate and regenerated TEMPO-oxidized cellulose model surfaces as a porous substrate. Particularly in the latter case, cellulose fibers were oxidized via TEMPO-mediated oxidation to a charge density of 629 ± 6 μmol/g, dissolved and then regenerated in MilliQ water. [28,29].

QCM-D is a gravimetric technique used to investigate the adsorbed amount (Γ_{QCM}) in combination with the associated water resulting in a viscoelastic perspective of the adsorbed layer, whereas SPAR, being a reflectometric technique (Figure S11), excludes the water, thus providing information only about the adsorbed amount of nanolatexes (Γ_{SPAR}). [25,26] By combining the results from both techniques it is possible to obtain crucial

Table 2
Physicochemical properties of nanolatexes synthesized by RAFT-mediated PISA.

Samples	p(%) [a]	M_n(g/mol) [b]	D_{SEM}(nm) [c]	D_H(nm) [d]	*PdI* [d]	ζ(mV) [d]	*Charge density*		T_g(°C) [f]
							μmol/g [e]	*μmol/m²*	
D_7-M_{100}	83	9850	37.5 ± 7.4	43.3 ± 3.3	0.12 ± 0.01	32.1 ± 1.0	327 ± 28	2.8 ± 0.3	115.0 ± 2.1
D_{15}-M_{200}	85	19,660	30.9 ± 8.2	36.5 ± 0.6	0.07 ± 0.01	62.1 ± 1.3	601 ± 61	4.3 ± 0.6	123.2 ± 0.7
D_{15}-M_{500}	84	44,690	56.3 ± 7.5	68.0 ± 1.2	0.06 ± 0.01	59.5 ± 2.4	342 ± 25	4.6 ± 0.5	124.5 ± 0.6
D_{25}-M_{200}	86	21,458	31.9 ± 6.8	44.9 ± 1.7	0.07 ± 0.02	52.7 ± 1.5	931 ± 144	8.2 ± 1.8	125.9 ± 0.7

[a] Monomer (MMA) conversion calculated from equation S2.
[b] Polymer molecular weight was calculated from equation S4.
[c] Diameter of nanolatexes measured by FE-SEM on spin-coated silica substrates.
[d] Hydrodynamic diameter, polydispersity index and zeta potential measured by DLS with 0.1 wt% dispersion in deionized water.
[e] Charge density measured by PET.
[f] Glass transition temperature obtained by DSC.

information about the adsorption and morphological relaxation of the nanolatexes and substrate during the adsorption process.

In general, Γ_{SPAR} follows a trend influenced by the charge density of the nanolatexes (Fig. 2, Table 3). For silica, the lowest Γ_{SPAR} was obtained when the charge was 931 μmol/g and the highest for 327 μmol/g, corresponding to D_{25}-M_{200} and D_7-M_{100}, respectively. It is expected that the nanolatexes can be more closely packed when their charge density is lower since their interparticle double layer repulsion will also be lower. [9] The range and magnitude of the potential field around adsorbed nanolatexes are affected by the charge compensation between the substrate and nanolatexes. The ideal adsorption scenario to reach a close packing requires two features: i) the nanolatex is small enough so that all charges can be reached and compensated by the charge of the surface, and ii) the local amount of charged groups of the surface is similar or higher than that of the nanolatex so that all charged groups of the nanolatex are compensated, leaving no excess charge to locally reverse the sign of the potential that would otherwise repel other incoming nanolatex. These features are illustrated in Fig. 3a, where the top left illustration shows the best scenario. [9] Charges on nanolatexes with a diameter larger than the charge correlation distance, i.e., the Debye length, can be too far away to be compensated by the surface charge and this will also lead to a local reversal of the surface potential (Fig. 3a bottom). The exact correlation distance at the interface is unknown, but it should be smaller than the calculated 60–100 nm (Table S4) in these nanolatex solutions since the charge concentration is higher at the interface. A 70 nm nanolatex sitting on the surface should thus be difficult to compensate, at least the charged groups on top of it. Raising this discussion is essential, and it calls for more theoretical and experimental studies to understand the microenvironment and how it influences nanoparticle adsorption.

The charge density of the polymer shell also influences the morphology of the contact zone to the surface. Fig. 4 conceptualizes the hypothetical difference between nanolatexes with low and high charge. In the former case (Fig. 4 top), the charges are fully compensated so that the nanolatexes and the shell polymers collapse into a strong and close contact. In the latter case (Fig. 4 bottom), the polymer shell has many uncompensated charges resulting in a swollen zone that prevents close contact due to the osmotic pressure preventing the collapse onto the surface, as indicated by the trapped water in Table 4. The latter scenario would lead to a weak contact zone with higher hydration and more mobile nature. Ideal compatibilization would be described by a sufficient contact between the nanolatex and the substrate and achieved by 1:1 charge compensation (Figure S19), which, as later shown, also helps to dehydrate the cellulose. Additionally, since the projected charge density of the regenerated TEMPO-oxidized cellulose model surfaces (~11 μmol/m^2) and silica (~0.5 μmol/m^2) are higher and lower than the charge density of the nanolatexes (2–8 μmol/m^2), the nanolatex charge undercompensates the TEMPO-oxidized cellulose surface (Figure S19). Thus, A surface with 3D distribution of charged groups is more favorable for high adsorption.

In the case of regenerated TEMPO-oxidized cellulose model surfaces, the highest Γ_{SPAR} was obtained from D_{15}-M_{500} and the lowest from D_{25}-M_{200} (Fig. 2b). However, the Γ_{SPAR} values for cellulose are

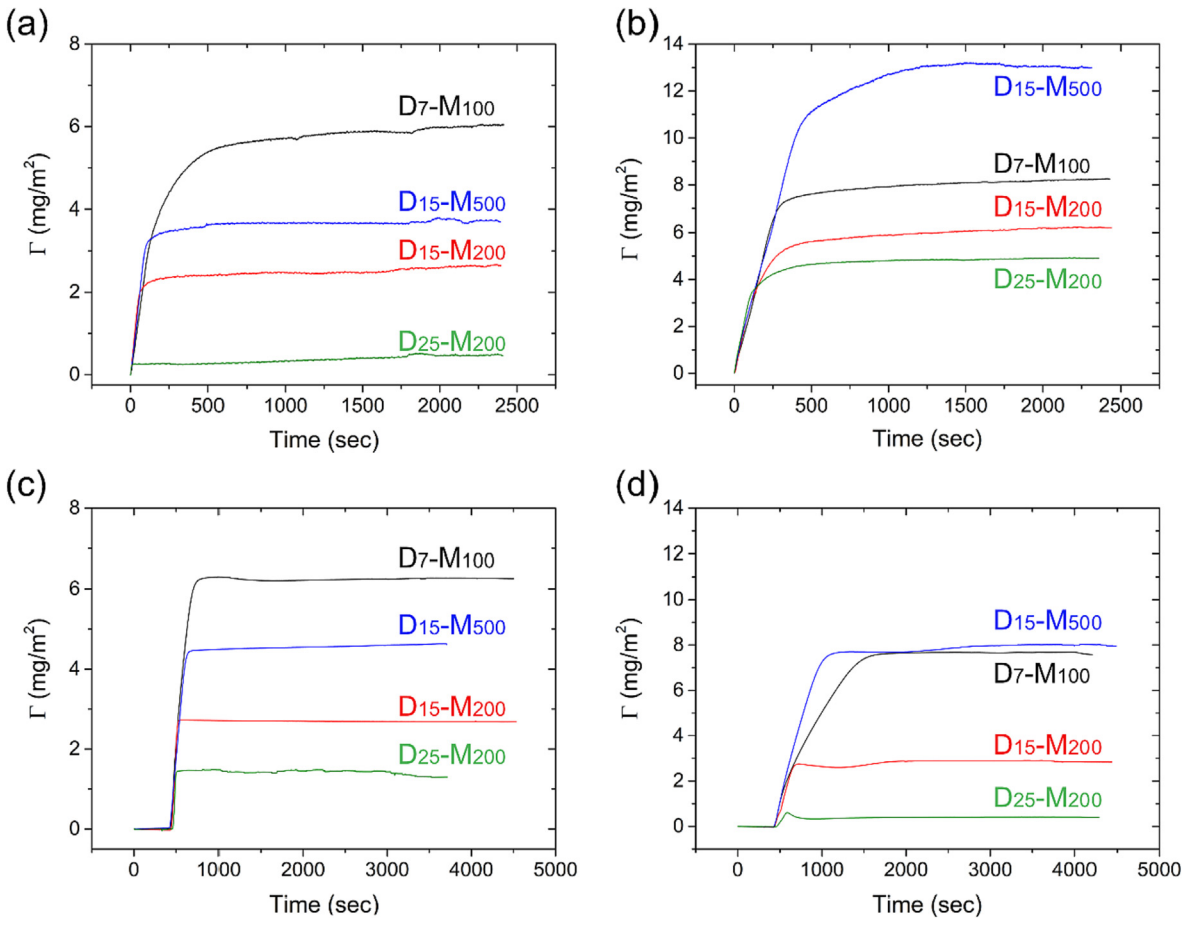

Fig. 2. The adsorbed amount of nanolatexes onto silica (a, c) and regenerated TEMPO-oxidized cellulose model surfaces (b, d) obtained from SPAR (top) and QCM-D (bottom); D_7-M_{100} (black line), D_{15}-M_{200} (red line), D_{15}-M_{500} (blue line) and D_{25}-M_{200} (green line). (For interpretation of the references to colour in this figure legend, the reader is referred to the web version of this article.)

Table 3
Adsorption characteristics of nanolatexes on silica and regenerated TEMPO-oxidized cellulose model surfaces obtained from SPAR and QCM-D.

Samples	Silica surface			Regenerated TEMPO-oxidized cellulose model surface		
	Γ_{SPAR}(mg/m^2) [a]	Γ_{QCM}(mg/m^2) [b]	$\Delta D \times 10^{6}$ [b]	Γ_{SPAR}(mg/m^2) [a]	Γ_{QCM}(mg/m^2) [b]	$\Delta D \times 10^{6}$ [b]
D_7-M_{100}	6.15 ± 0.43	6.28 ± 0.04	2.94 ± 0.10	8.43 ± 0.80	7.53 ± 0.15	2.60 ± 0.71
D_{15}-M_{200}	2.59 ± 0.09	2.72 ± 0.05	1.81 ± 0.59	6.26 ± 0.13	2.80 ± 0.04	−1.41 ± 0.30
D_{15}-M_{500}	3.44 ± 0.46	4.43 ± 0.26	5.84 ± 0.22	13.34 ± 1.11	7.82 ± 0.21	2.72 ± 1.02
D_{25}-M_{200}	0.72 ± 0.42	1.48 ± 0.08	0.92 ± 0.30	5.66 ± 0.95	0.404 ± 0.004	−2.77 ± 0.18

[a] Adsorbed amount obtained from SPAR (equation (1)).
[b] Adsorbed amount (equation (2)) and dissipation (equation (3)) obtained from QCM-D.

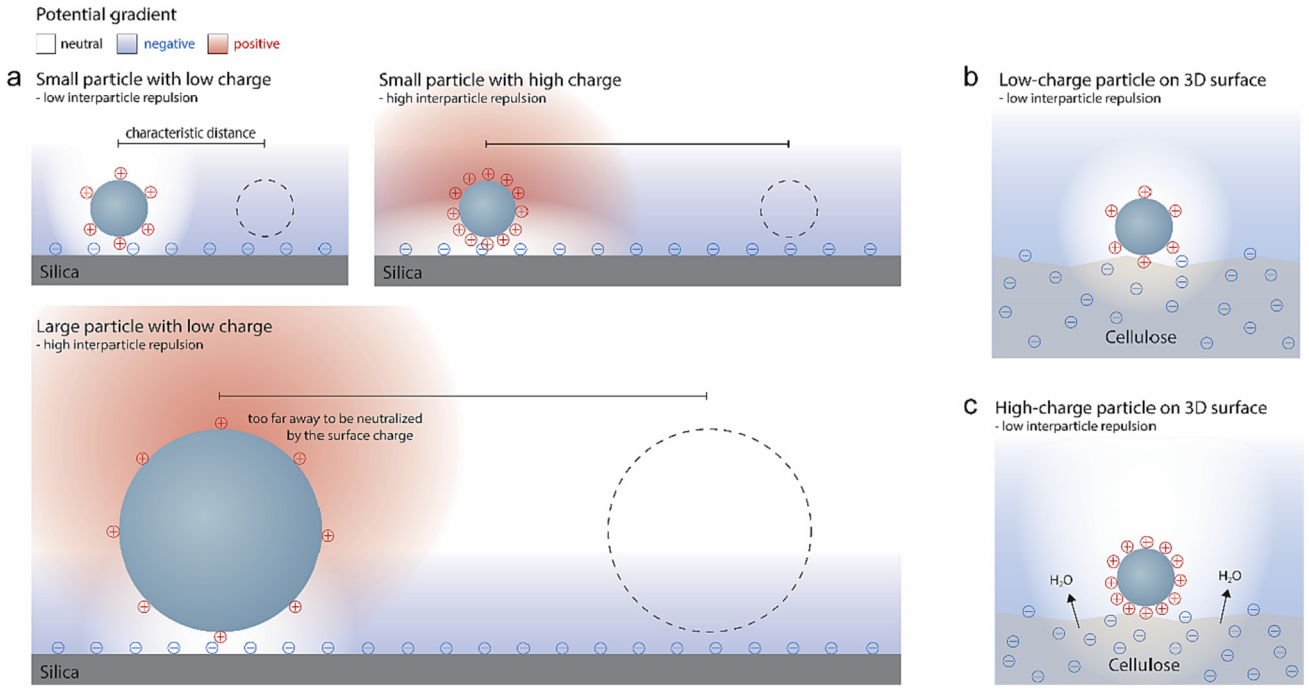

Fig. 3. Schematic representation of the potential field surrounding small and large nanolatexes of different charge densities when adsorbed onto silica (a) and cellulose (b, c). The sketch is not to scale.

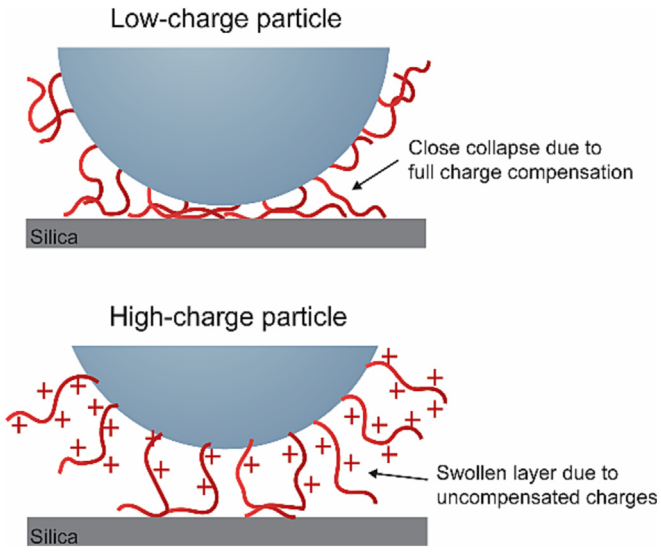

Fig. 4. Schematic representation of the influence of low (top) and high (bottom) charged nanolatexes when adsorbed onto silica. The sketch is not to scale.

generally higher than for silica. This result is a consequence of the vertical (volumetric) distribution of charges in the case of cellulose, meaning that it has more charges per surface area available to compensate the charge of the nanolatex, as illustrated in Fig. 3b. This behavior has also been reported when adsorbing polyelectrolytes on regenerated TEMPO-oxidized cellulose model surfaces of greater thickness than in this work. [27] The charge of the nanolatex can compensate charges deep inside the cellulose at distances in the order of the Debye length. The difference between the Γ_{SPAR} of the nanolatexes when comparing the two substrates is the effect of both charge density and size (Figure S14). Specifically, D_7-M_{100} and D_{15}-M_{500} compete for the highest adsorbed mass when only the charge density is considered the driving force. When the size is accounted for, it is expected for D_{15}-M_{500} to exhibit the highest adsorbed mass since it is the largest and heaviest nanolatex. However, heavier and larger nanolatexes may have difficulties adsorbing due to the small contact area in relation to the volume of the nanolatex, i.e. balance between inertia and capturing force.

The results from QCM-D show that the same trends are observed for both investigated surfaces (Fig. 2c and 2d). On silica, Γ_{QCM} is very similar to Γ_{SPAR}. On the contrary, the values of Γ_{QCM} for the regenerated TEMPO-oxidized cellulose model surfaces are lower compared to their respective Γ_{SPAR}. This difference is because QCM-D considers the water uptake or release. According to the literature, cellulose surfaces can deswell when the charges are neu-

tralized by an adsorbing moiety, as illustrated in Fig. 3c, reflected in a lower mass adsorbed or even overall mass loss. [36,37] This deswelling is also apparent in this study and can be observed by the negative sign of the dissipation (ΔD) values listed in Table 3 (Figure S12). The complexity of the adsorption onto silica and cellulose is further highlighted when plotting the ΔD as a function of change in frequency (Figure S13). It can be observed that the adsorption obeys a linear trend on silica, meaning that each adsorbed nanolatex contributes to a constant change in the viscoelastic response. On the contrary, on cellulose, the relationship is much more intricate, with the viscoelastic response changing throughout the adsorption due to the change in viscoelastic properties of the cellulose during deswelling.

Crucial parameters can be calculated by combining the results from SPAR and QCM-D through equations S7-S12. The trapped water on the substrate is also included in QCM-D, and by combining Γ_{SPAR} and Γ_{QCM} through equation S11, the amount of associated water (x) can be calculated (Table 4). For the case of silica, all values are positive, and the highest amount of trapped water within error is observed for D_{25}-M_{200}. However, x is negative for the adsorption onto regenerated TEMPO-oxidized cellulose model surfaces, which makes it an indisputable indicator of the apparent deswelling, also verified by other studies. [36,37] It should be noted that in this case, the amount of trapped water for cellulose can only be used qualitatively since the amount of water associated with the nanolatexes cannot be accounted for. Negative values of x are the minimum amount of water released during deswelling. However, since x for adsorption onto silica is relatively low, the error in x for adsorption onto cellulose is expected to be small.

The adsorption rate was investigated theoretically and experimentally to understand the adsorption phenomena. In the former case, the theoretical flux of adsorption (J) was calculated according to equation S12. The experimental flux was obtained from the initial slope of the SPAR adsorption curves (Table S3), and it was correlated to the theoretical, allowing assessment of the adsorption efficiency in SPAR (Table 4). Although the adsorption efficiency ranges between 30 and 50 % for both surfaces, D_{15}-M_{500} seems to adsorb more efficiently, reaching 60 % for the silica surface. This difference could be because the number of nanolatexes is less in the initial dispersion, and thus there is less competition when adsorbing on the surface (*SI* part 11).

The surfaces used in QCM-D were subsequently imaged by FE-SEM (Fig. 5). The highest coverage of the substrate was observed for the regenerated TEMPO-oxidized cellulose model surfaces. This was also expected based on the calculated volume (Φ_V) and area (Φ_A) coverage (Table 3). In brief, on both substrates, according to Φ_V, the highest coverage was observed for the nanolatex with the lowest surface charge density, i.e., D_7-M_{100}, and the lowest coverage for the nanolatex with the highest charge density, i.e., D_{25}-M_{200}.

The adsorption onto silica surfaces was also measured at different electrolyte concentrations. The double layer repulsion between the nanolatexes is screened by increasing salt concentration, allowing them to pack closer. [9] This will naturally enhance the adsorbed amount of nanolatexes while 100 mM is low enough to ensure that charge exchange is still the main driving force for adsorption. [24] D_{25}-M_{200} was diluted at 0.025 g/L with 1, 10 and 100 mM NaCl. As seen in *SI* part 12, Γ_{QCM} increased from 1.5 to 5.0 mg/m^2 when going from 1 to 100 mM NaCl (Table S5). This increase is observed in the FE-SEM images (Figure S21). Thus by tuning the size, charge density, and electrolyte concentration during adsorption, it is possible to optimize the nanolatexes and the conditions for a specific surface.

An indirect way to evaluate the successful modification of a substrate with hydrophilic nanolatexes is by measuring the contact

Table 4
Characteristics of the adsorbed nanolatex layer onto silica and regenerated TEMPO-oxidized cellulose model surfaces.

Samples	Silica surface				Regenerated TEMPO-oxidized cellulose model surface			
	x [a]	Adsorption efficiency (%) [b]	Φ_V(%) [c]	Φ_A(%) [c]	x [a] *	Adsorption efficiency (%) [b]	Φ_V(%) [c]	Φ_A(%) [c]
D_7-M_{100}	0.05 ± 0.04	32.7 ± 0.3	6.2 ± 0.4	9.3 ± 0.9	−0.12 ± 0.12	36.0 ± 2.5	8.4 ± 0.8	12.6 ± 1.7
D_{15}-M_{200}	0.05 ± 0.02	39.2 ± 2.7	3.0 ± 0.1	4.5 ± 0.2	−1.28 ± 0.39	33.2 ± 0.6	7.3 ± 0.1	11.0 ± 0.2
D_{15}-M_{500}	0.23 ± 0.08	59.7 ± 0.3	2.0 ± 0.3	3.0 ± 0.6	−0.70 ± 0.14	47.3 ± 6.9	7.6 ± 0.6	11.4 ± 1.2
D_{25}-M_{200}	0.53 ± 0.36	31.2 ± 1.7	0.7 ± 0.4	1.1 ± 0.8	−13.00 ± 3.13	47.2 ± 7.7	5.7 ± 1.0	8.6 ± 2.1

[a] Mass fraction of trapped water calculated from equation S11.
[b] Calculated by comparing the theoretical flux of adsorption (J, equation S12) and the experimental flux obtained from the initial slope of adsorption of the SPAR curves.
[c] Volume and area coverage estimated by equations S7 and S10, respectively.
* Trapped water values for cellulose are only used as a qualitative comparison.

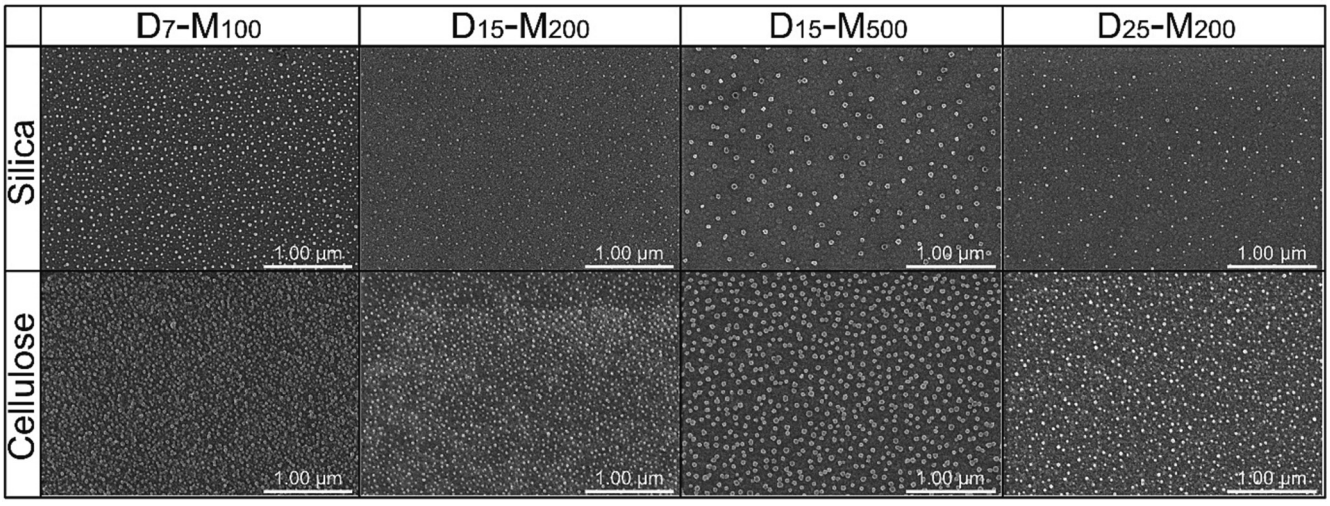

Fig. 5. FE-SEM images of adsorbed nanolatexes on silica (top) and regenerated TEMPO-oxidized cellulose model surfaces (bottom). The scale bar is 1 µm for all images.

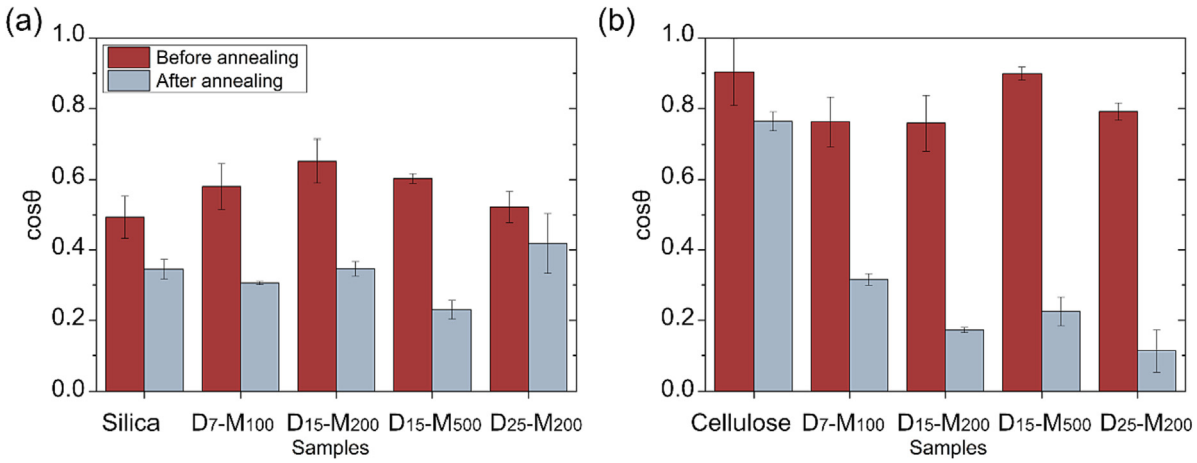

Fig. 6. Contact angle measurements of modified silica (a) and regenerated TEMPO-oxidized cellulose model surfaces (b); before (red bars) and after annealing at 150 °C for 5 h (grey bars); cos(90°) = 0 (nonwetting) and cos(0°) = 1 (complete wetting). (For interpretation of the references to colour in this figure legend, the reader is referred to the web version of this article.)

angle against water. Based on the contact angle, the *cosθ* ranges between 0 and 1, where 1 means complete wetting of the surface and indicates that the substrate is hydrophilic while 0 describes a hydrophobic substrate. The *cosθ* of the silica substrates was slightly higher than the pristine substrate after the adsorption of nanolatexes due to their hydrophilic shell, whereas the opposite behavior was observed for the regenerated TEMPO-oxidized cellulose model surfaces (Fig. 6). In the case of D_{25}-M_{200} adsorbed onto the silica surfaces in the presence of NaCl, the *cosθ* was increased by increasing salt concentration (Table S5). This behavior can be explained by the increasing number of hydrophilic nanolatexes adsorbed onto the surface.

The adsorbed nanolatexes comprised of a high T_g PMMA core have previously been shown to promote hydrophobicity upon annealing. [14,15] Different protocols exist for annealing such nanolatexes on cellulose surfaces at higher temperatures. For instance, in a previous study involving high T_g latexes, 150 °C was used as the annealing temperature for 1 and 8 h. [30] In our case, to ensure the complete annealing of the nanolatexes while at the same time considering the sensitivity of regenerated TEMPO-oxidized cellulose model surface under these conditions, the same temperature was used, but the annealing time was reduced to 5 h. [38] Hydrophobicity was promoted when the substrates were annealed under these conditions (Fig. 6). For the case of silica, a decrease in *cosθ* was observed whereas the most significant difference was observed for regenerated TEMPO-oxidized cellulose model surfaces. Approximately a 4-fold decrease in *cosθ* was observed, which indicates the annealing into a hydrophobic layer of PMMA. [30] This change due to thermal treatment was also imaged by FE-SEM (Figures S21, S22), showing black spots indicating the softened nanolatexes on silica, whereas a relatively smoother surface is observed on cellulose.

4. Conclusions

This work addresses the lack of fundamental understanding of how the size and charge density influence the adsorption of versatile cationically charged nanolatexes synthesized via RAFT-mediated PISA. The influence of morphology of the substrate was also investigate to present a broad description of nanolatex adsorption. Nanolatexes were adsorbed onto silica and negatively charged, regenerated TEMPO-oxidized cellulose model surfaces, respectively, and their adsorption was studied by SPAR and QCM-D. It was found that the charge density of the nanolatexes is the governing parameter for the adsorbed amount onto silica, whereby increasing the charge density of the nanolatexes decreases the adsorbed amount onto silica due to overcompensation and interparticle repulsion. In the case of regenerated TEMPO-oxidized cellulose model surfaces, even highly charged nanolatexes cannot compensate all the charges on the surface, and the adsorption is greater. Too large particles have charged groups that are outside the reach of the surface and can still lead to interparticle repulsion due to the reversal of the surface potential.

NaCl(aq) was also used to promote the adsorbed amount of nanolatexes onto silica by screening the double layer repulsion between particles. Previously published works focused on investigating surface coverage for different particle sizes [10] or the combined effect of size and charge density on the adsorption. [8,14,15,22] In particular, it was found that apart from the influence of the T_g of the core polymer, the simultaneous decrease in charge density and increase in size were necessary to reach the optimum adsorbed amount. However, detailed studies are rare since the synthesis of well-defined particles with decoupled sizes and charge densities is challenging. The RAFT-mediated PISA route provides an excellent platform for developing nanolatexes with decoupled charge density and size to study the influence of these parameters further.

The experimental results agree qualitatively with theoretical electrostatic mean field models, [9] and can be used to tailor nanolatexes for a specific substrate by tuning size, charge density and electrolyte concentration during adsorption. This work expanded our understanding of the critical parameters of adsorption, which is essential for designing compatibilizer systems for cellulose composites or other soft substrates.

The modified substrates were also annealed, exposing the hydrophobic character of the PMMA-core of the nanolatexes to make the substrate hydrophobic as a method for compatibilization. [14,15] This work aims to increase our understanding on the adsorption of nanolatexes that can be synthesized in water and exhibit properties on-demand depending on the substrate targeted for modification. The long-term goal is to use these results to develop a platform for tailoring the compatibility between differently charged surfaces and matrixes in composite material applications.

CRediT authorship contribution statement

Alexandros Efraim Alexakis: Conceptualization, Methodology, Validation, Formal analysis, Investigation, Data curation, Writing – original draft, Visualization. **Maria Rosella Telaretti Leggieri:** Val-

idation, Writing – review & editing. **Lars Wågberg:** Conceptualization, Methodology, Writing – review & editing. **Eva Malmström:** Conceptualization, Methodology, Resources, Writing – review & editing, Project administration, Funding acquisition. **Tobias Benselfelt:** Methodology, Formal analysis, Writing – review & editing, Visualization.

Data availability

Data will be made available on request.

Declaration of Competing Interest

The authors declare that they have no known competing financial interests or personal relationships that could have appeared to influence the work reported in this paper.

Acknowledgements

The authors acknowledge funding from the Knut and Alice Wallenberg Foundation (KAW) through the Wallenberg Wood Science Center and a personal fellowship for Tobias Benselfelt.

Appendix A. Supplementary material

Supplementary data to this article can be found online at https://doi.org/10.1016/j.jcis.2022.12.038.

References

[1] T. Li, C. Chen, A.H. Brozena, J.Y. Zhu, L. Xu, C. Driemeier, J. Dai, O.J. Rojas, A. Isogai, L. Wågberg, L. Hu, Nature 590 (2021) 47–56.
[2] W. Liu, K. Liu, H. Du, T. Zheng, N. Zhang, T. Xu, B. Pang, X. Zhang, C. Si, K. Zhang, Nano-Micro Lett. 14 (2022) 104.
[3] G. Siqueira, J. Bras, A. Dufresne, Polymers-Basel 2 (2010) 728–765.
[4] K. Missoum, M.N. Belgacem, J. Bras, Materials 6 (2013) 1745–1766.
[5] M.V. Kiriakou, A.S. Pakdel, R.M. Berry, T. Hoare, M.A. Dubé, E.D. Cranston, ACS Materials Au 2 (2022) 176–189.
[6] E.K. Oikonomou, K. Golemanov, P.-E. Dufils, J. Wilson, R. Ahuja, L. Heux, J.-F. Berret, ACS Appl. Polym. Mater. 3 (2021) 3009–3018.
[7] C. Jiménez Saelices, M. Save and I. Capron, *Polym Chem-Uk*, 2019, **10**, 727-737.
[8] J. Engström, T. Benselfelt, L. Wågberg, F. D'Agosto, M. Lansalot, A. Carlmark, E. Malmström, Nanoscale 1 (2019) 4287–4302.
[9] Z. Adamczyk, P. Warszynski, Adv. Colloid Interfac 63 (1996) 41–149.
[10] E. Tellechea, D. Johannsmann, N.F. Steinmetz, R.P. Richter, I. Reviakine, Langmuir 25 (2009) 5177–5184.
[11] Z. Adamczyk, K. Jaszczolt, A. Michna, B. Siwek, L. Szyk-Warszynska, M. Zembala, Adv. Colloid Interfac 118 (2005) 25–42.
[12] D. Kosior, M. Gvaramia, L.R.J. Scarratt, P. Maroni, G. Trefalt, M. Borkovec, Soft Matter 17 (2021) 6212–6224.
[13] J. Engström, M.S. Reid, E.E. Brotherton, E. Malmström, S.P. Armes, F.L. Hatton, Polym. Chem.-Uk (2021) 12.
[14] J. Engström, F.L. Hatton, L. Wågberg, F. D'Agosto, M. Lansalot, E. Malmström, A. Carlmark, Polym. Chem.-Uk 8 (2017) 1061–1073.
[15] L. Carlsson, A. Fall, I. Chaduc, L. Wågberg, B. Charleux, E. Malmström, F. D'Agosto, M. Lansalot, A. Carlmark, Polym. Chem.-Uk 5 (2014) 6076–6086.
[16] I.R. Quevedo, A.L.J. Olsson, N. Tufenkji, Environ. Sci. Tech. 47 (2013) 2212–2220.
[17] M. Lansalot, Rieger, J. and D'Agosto, F., in *Macromolecular Self-assembly*, John Wiley & Sons, Inc., 2016, 33-82.
[18] I. Chaduc, W.J. Zhang, J. Rieger, M. Lansalot, F. D'Agosto, B. Charleux, Macromol. Rapid Comm. 32 (2011) 1270–1276.
[19] A.M. dos Santos, J. Pohn, M. Lansalot, F. D'Agosto, Macromol. Rapid Comm. 28 (2007) 1325–1332.
[20] C.J. Ferguson, R.J. Hughes, D. Nguyen, B.T.T. Pham, R.G. Gilbert, A.K. Serelis, C.H. Such, B.S. Hawkett, Macromolecules 38 (2005) 2191–2204.
[21] N.J.W. Penfold, J. Yeow, C. Boyer, S.P. Armes, ACS Macro Lett. 8 (2019) 1029–1054.
[22] F.L. Hatton, M. Ruda, M. Lansalot, F. D'Agosto, E. Malmström, A. Carlmark, Biomacromolecules 17 (2016) 1414–1424.
[23] V. Ladmiral, A. Charlot, M. Semsarilar, S.P. Armes, Polym. Chem.-Uk 6 (2015) 1805–1816.
[24] J. Fu, J.B. Schlenoff, J. Am. Chem. Soc. 138 (2016) 980–990.
[25] N. Alipoormazandarani, T. Benselfelt, L.Y. Wang, X.J. Wang, C.L. Xu, L. Wågberg, S. Willfor, P. Fatehi, Acs Appl. Mater. Inter. 13 (2021) 26308–26317.
[26] T. Benselfelt, E.D. Cranston, S. Ondaral, E. Johansson, H. Brumer, M.W. Rutland, L. Wågberg, Biomacromolecules 17 (2016) 2801–2811.
[27] T. Benselfelt, T. Pettersson, L. Wågberg, Langmuir 33 (2017) 968–979.
[28] T. Saito, M. Hirota, N. Tamura, S. Kimura, H. Fukuzumi, L. Heux, A. Isogai, Biomacromolecules 10 (2009) 1992–1996.
[29] T. Saito, S. Kimura, Y. Nishiyama, A. Isogai, Biomacromolecules 8 (2007) 2485–2491.
[30] A.E. Alexakis, J. Engström, A. Stamm, A.V. Riazanova, C.J. Brett, S.V. Roth, P.O. Syren, L. Fogelström, M.S. Reid, E. Malmström, Green Chem. 23 (2021) 2113–2122.
[31] Scandinavian Pulp, Sweden: Scandinavian Pulp, Paper and Board Testing Committee.
[32] J.C. Dijt, M.A.C. Stuart, G.J. Fleer, Adv. Colloid Interfac 50 (1994) 79–101.
[33] Z.P.G. Sauerbrey, Z. Phys. 155 (1959) 206–222.
[34] C. Aulin, I. Varga, P.M. Claessont, L. Wågberg, T. Lindström, Langmuir 24 (2008) 2509–2518.
[35] X. Dong, H. Bao, K. Ou, J. Yao, W. Zhang, J. He, Fibers Polym. 16 (2015) 1478–1486.
[36] L.E. Enarsson, L. Wågberg, Biomacromolecules 10 (2009) 134–141.
[37] S.M. Notley, PCCP 10 (2008) 1819–1825.
[38] H. Fukuzumi, T. Saito, Y. Okita, A. Isogai, Polym. Degrad. Stab. 95 (2010) 1502–1508.